Elastic full-waveform inversion with spatial probabilistic petrophysical constraints

Odette Aragao & Paul Sava

Center for Wave Phenomena and Dept. of Geophysics, Colorado School of Mines, Golden CO 80401
aquinodearagao@mines.edu

ABSTRACT

Full-waveform inversion (FWI) produces high resolution models of subsurface properties by exploiting both the dynamics and the kinematics of the observed seismic waveforms. However, the feasibility of FWI depends on a number of well-known factors, such as the quality of inversion starting models and the data frequency content, given that the inverse problem is highly non-linear and its solution is non-unique. Particularly, when one considers an elastic wave equation for wavefield extrapolation, if the objective function is purely based on the misfit between modeled and observed data, the quality of the inverted models is hampered by artifacts produced by interparameter crosstalk, and some combinations of model components may even be lithologically implausible. In light of the aforementioned problems, we propose an augmented objective function for elastic full-waveform inversion (EFWI), which exploits both the data misfit and the consistency of the seismic data with available petrophysical information in the studied area. We classify the petrophysical data considering spatial distribution patterns, e.g. depth trends, and compute multiple probability density functions to formulate a penalty term, incorporated explicitly in the inversion objection function. This penalty confines the inverted models to a feasible petrophysical space, while allowing the conventional data misfit term to control the specific distribution of subsurface parameters.

Key words: full-waveform inversion, elastic, petrophysics

1 INTRODUCTION

Wavefield tomography is a state-of-the-art technique used to estimate physical properties of the subsurface from recorded data. It has multiple uses and broad applicability in seismic exploration and subsurface characterization. This technique exploits wavefield propagation in order to generate subsurface models by solving an inverse problem. One can implement tomography in the data domain (pre-migration) or in the image domain (post-migration).

Full-waveform inversion (FWI), a data domain wavefield tomography technique, is a widely used tool for building high-resolution subsurface models (Tarantola, 1984). FWI operates by iteratively updating an initial model, while minimizing the difference between the observed and the predicted data. When using the adjoint state method (Plessix, 2006), the subsurface property updates are obtained by cross-correlating the forward-propagated source wavefield and the backward-propagated adjoint wavefield, which is extrapolated using the misfit between the observed and simulated data. The method has great ability to produce high resolution models, by exploiting kinematic and dynamic properties of the extrapolated wavefields.

However, FWI suffers from a series of well-identified problems (Virieux and Operto, 2009). The objective function is multimodal, and thus the inverse problem is non-linear and its solution is non-unique. Additionally, the inversion strongly depends on the feasibility of the starting model, such that if the initial model is not sufficiently accurate, FWI is prone to cycle skipping, which may trap the inversion in local minima. Furthermore, implementations using an elastic wave equation, such as elastic full-waveform inversion (EFWI), estimate multiple models of subsurface parameters, increasing the number of model combinations that can equally explain the data, thus leading to a larger domain of ambiguity (Operto et al., 2013). Moreover, different elastic properties may be coupled as they have similar radiation patterns and updates of one parameter could leak into others, an effect

known as interparameter trade-off or crosstalk. Lastly, some components of the recovered model parameters can be lithologically implausible or even impossible (e.g., negative Poisson ratio), and not represent feasible lithological units. This effect is due to the fact that model parameters are updated simultaneously, but independently during the EFWI process.

An option to reduce the number of possible solutions for the ill-posed FWI problem is adding a model regularization term to the objective function, e.g. first- and second-order Tikhonov regularization or total variation (TV) techniques (Guitton, 2012; Asnaashari et al., 2013; Zhang et al., 2018; Zhang and Alkhalifah, 2019). However, even when incorporating a model regularization term in the FWI object function, the model parameters are still updated independently, and may represent unfeasible lithologies. Additionally, these regularization methods operate in the spatial domain and their efficiency strongly relies on accurate geological information about the entire studied region while prior petrophysical information derived from well logs or other sources characterizes the model only at sparse locations.

Aragao and Sava (2020a) exploit the petrophysical data in the model parameter space as a penalty term for the objective function to impose explicit limitations on what models are acceptable as solutions to the inverse problem, thus guiding models toward realistic lithology. They use probability density function (PDF) in order to constrain EFWI without defining specific analytic relationships between the elastic properties, in order to avoid assuming explicit and potentially inaccurate petrophysical relations among them. Aragao and Sava (2020b) adapts the approach of Aragao and Sava (2020a) by building a penalty term using multiple PDFs, each representing a different lithological unit. Both works demonstrate that explicitly imposing probabilistic petrophysical penalties increase the robustness of EFWI, as it leads to reliable elastic models that are geologically plausible, while reducing the non-linearity and ill-posed nature of FWI and mitigating artifacts produced by interparameter crosstalk.

Here, we use a strategy similar to that of Aragao and Sava (2020b) and propose to use petrophysical penalties defined based on different PDFs. We consider each PDF as spatial distribution patterns characterizing the petrophysical data, e.g. lithological trends with depth as indicated by well-logs. Additionally, when well logs are available at various spatial locations, we can use multiple PDFs based on the spatial location of the wells. In this way, we can incorporate in the penalty term all the available petrophysical information that may indicate the occurrence of distinct lithological units as a function of depth and well location.

We illustrate the efficiency of the proposed framework with a synthetic example. We show how the probabilistic petrophysical penalty term based on different depth trends and spatial locations can deliver models with high resolution that are closer to the true models compared with the cases of unconstrained inversion or when a single PDF is used to characterize the entire inverted model.

2 THEORY

Consider the isotropic elastic wave equation,

$$\rho\ddot{\mathbf{u}} - \lambda[\nabla(\nabla\cdot\mathbf{u})] - \mu\left[\nabla\cdot\left(\nabla\mathbf{u}+\nabla\mathbf{u}^T\right)\right] = \mathbf{f}, \tag{1}$$

where $\mathbf{u}(e,\mathbf{x},t)$ is the elastic displacement, $\mathbf{f}(e,\mathbf{x},t)$ is the source function, $\lambda(\mathbf{x})$ and $\mu(\mathbf{x})$ are the Lamé parameters, $\rho(\mathbf{x})$ is the density, and e, $\mathbf{x}$ and t are, respectively, the experiment index, space coordinates and time. We solve the FWI problem by minimizing an objective function $\mathcal{J}$ composed by two terms: one calculates the L2-norm of the misfit between the observed and predicted data ($\mathcal{J}_D$), and the other penalizes the models using petrophysical data.

Aragao and Sava (2020a) use all the available petrophysical data to determine a single PDF in order to compute the petrophysical penalty $\mathcal{J}_P$. The PDF is represented in the petrophysical space by coordinates $\mathbf{p} = \{\lambda_p, \mu_p\}$, and the components of the model parameters are represented by the vector $\mathbf{m}(\mathbf{x}) = \{\lambda(\mathbf{x}), \mu(\mathbf{x})\}$. They use the probability density $f(\mathbf{p})$ to determine the distance $D(\mathbf{m})$ from $\mathbf{m}$ to the entire distribution as

$$\frac{1}{D(\mathbf{m})} = \sum_{\mathbf{p}} \frac{f(\mathbf{p})}{d(\mathbf{m},\mathbf{p})}, \tag{2}$$

where $d(\mathbf{m},\mathbf{p})$ corresponds to the distance from any given model represented by coordinates $\mathbf{m}$ to any point in the petrophysical space:

$$d(\mathbf{m},\mathbf{p}) = \|\mathbf{m}-\mathbf{p}\|_2. \tag{3}$$

Finally, considering a scalar parameter a that determines the strength of $\mathcal{J}_P$ in the objective function, Aragao and Sava (2020a) define the penalty term as

$$\mathcal{J}_P = a \sum_{\mathbf{m}} D(\mathbf{m}). \tag{4}$$

The gradients of $\mathcal{J}_P$ with respect to the model parameters λ and μ are given by

$$\begin{bmatrix} \dfrac{\partial \mathcal{J}_P}{\partial \lambda} \\ \dfrac{\partial \mathcal{J}_P}{\partial \mu} \end{bmatrix} = a \begin{bmatrix} D^2(\mathbf{m}) \sum_{\mathbf{p}} \dfrac{f(\mathbf{p})(\lambda - \lambda_p)}{d^3(\mathbf{m},\mathbf{p})} \\ D^2(\mathbf{m}) \sum_{\mathbf{p}} \dfrac{f(\mathbf{p})(\mu - \mu_p)}{d^3(\mathbf{m},\mathbf{p})} \end{bmatrix}. \tag{5}$$

Aragao and Sava (2020b) propose to use multiple PDFs obtained by clustering petrophysical information when calculating the penalty term, such that each PDF represents a different lithological unit. Here we aim to use a similar approach, and take into account that subsurface formations may have spatial distribution patterns, e.g. depth trends, due to composition, porosity, pore-pressure, or compaction. Then, we classify the petrophysical data considering different spatial distribution patterns and compute multiple PDFs, depending on spatial location. We label this spatial-dependent petrophysical penalty $\mathcal{J}_T$, and proceed with an inversion strategy that resembles that defined by Aragao and Sava (2020a,b).

3 EXAMPLES

We illustrate our EFWI method with a synthetic example and compare inversions using (a) only the data misfit term $\mathcal{J}_D$, (b) the data misfit with the petrophysical penalty based on a single PDF $\mathcal{J}_P$, and (c) the data misfit with the petrophysical penalty based on multiple PDFs $\mathcal{J}_T$, each representing different depth trends.

The synthetic models shown in Figure 1 contain two positive Gaussian anomalies centered at $(0.6, 0.6)$ km and $(1.4, 1.4)$ km and two negative Gaussian anomalies centered at $(0.6, 1.4)$ and $(1.4, 0.6)$ km. There are 50 vertical displacement sources in a well at $x = 0.05$ km and a line of geophones at $x = 1.95$ km. We initiate the inversion with models of constant $\lambda = 10.4$ GPa and $\mu = 5.2$ GPa, which correspond to the background of the true models (Figure 1). We consider that prior petrophysical data from two wells located at $x = 0.6$ km $x = 1.4$ km are available and depicted in Figures 2. On the one hand, the data related to the first well (Figures 2a and 2b) indicates the occurrence of a positive anomaly above $z = 1.0$ km and a negative anomaly below $z = 1.0$ km. On the other hand, for the well logs depicted in Figure 2c and 2d, from $z = 0.0$ km to $z = 1.0$ km, we observe a negative anomaly, while from $z = 1.0$ km to $z = 2.0$ km, a positive anomaly is present. Therefore, we need to define 4 distributions given by different PDFs:

- f_1 using the well log at $x = 0.6$ km above $z = 1.0$ km, that corresponds to the green dots in Figure 3, to estimate the penalty for points of the models such that $x \in [0.0,\ 1.0]$ km and $z \in [0.0,\ 1.0]$ km;
- f_2 using the well log at $x = 0.6$ km below $z = 1.0$ km, that corresponds to the magenta dots in Figure 3, to estimate the penalty for points of the models such that $x \in [0.0,\ 1.0]$ km and $z \in [1.0,\ 2.0]$ km;
- f_3 using the well log at $x = 1.4$ km above $z = 1.0$ km, that corresponds to the yellow dots in Figure 3, to estimate the penalty for points of the models such that $x \in [1.0,\ 2.0]$ km and $z \in [0.0,\ 1.0]$ km;
- f_4 using the well log at $x = 1.4$ km below $z = 1.0$ km, that corresponds to the blue dots in Figure 3, to estimate the penalty for points of the models such that $x \in [1.0,\ 2.0]$ km and $z \in [1.0,\ 2.0]$ km.

Therefore, we calculate the penalty term for each point $\mathbf{m}$ in the updated model, depending on the spatial location of $\mathbf{m}$, using one of these four PDFs.

Figures 4a, 4b, 4c and 4d display the distance $D(\mathbf{m})$ and the gradient of $D(\mathbf{m})$ corresponding to f_1, f_2, f_3 and f_4, respectively. One can notice that when a point of coordinates $\mathbf{m}$ in the updated model is consistent with the distribution given by its correspondent PDF, $D(\mathbf{m})$ and its gradient are both zero. In this case, the data misfit $\mathcal{J}_D$ fully controls the inversion gradient for that point.

Figure 5 shows the recovered λ and μ models using the objective function $\mathcal{J}_D$. Without imposing any petrophysical penalty, the μ model has higher resolution than the λ model, which does not present anomalies with the same shape or magnitude as the

true λ model (Figure 1). Also, the recovered models depicted in Figure 5 are strongly hampered by spurious artifacts due to the trade-off between the elastic parameters, the limited acquisition coverage and the varying illumination.

Figure 6 shows the recovered λ and μ models using the objective function $\mathcal{J}_D + \mathcal{J}_P$. In this case, we use all the available petrophysical data (Figure 2) and build only a single PDF. Different from the inversion using only $\mathcal{J}_D$ (Figure 5), all anomalies have magnitude and shape closer to the true models (Figure 1). Additionally, the resolution of the inverted λ model is similar to that of the μ model. Furthermore, when adding the petrophysical penalty term, some artifacts related to the interparameter crosstalk are mitigated during the inversion.

Figure 7 shows the recovered λ and μ models using the objective function $\mathcal{J}_D + \mathcal{J}_T$. The inverted λ and μ models depicted in Figure 7 show fewer artifacts, have comparable resolution to each-other, and are closer to the true models (Figure 1) compared with the cases when we use the objective functions $\mathcal{J}_D$ (Figure 5) or $\mathcal{J}_D + \mathcal{J}_P$ (Figure 6).

4 CONCLUSIONS

We describe an approach to incorporate petrophysical information into the objective function of elastic full-waveform inversion by using a penalty term based on probability density functions (PDFs) that take into account spatial distribution of petrophysical properties. We demonstrate that defining multiple PDFs leads to inverted models that are closer to the true ones than inverted models obtained using a single PDF. This approach allows us to account for the fact that well logs can indicate that elastic properties may change substantially horizontally or vertically. We show that this technique guides the inversion to high-quality models, while mitigating interparameter crosstalk and steering inversion toward geologically plausible earth models that are consistent with the seismic data, as well as with the underlying petrophysics.

5 ACKNOWLEDGEMENTS

We acknowledge CAPES (Brazilian Federal Agency for Support and Evaluation of Graduate Education) for financial support. We thank the sponsors of the Center for Wave Phenomena (CWP) for additional support of this research. The synthetic example in this paper uses the Madagascar open-source software package (Fomel et al., 2013) freely available from http://www.ahay.org.

REFERENCES

Aragao, O., and P. Sava, 2020a, Elastic full-waveform inversion probabilistic petrophysical model constraints: Geophysics, **85**, no. 2, R101–R111.

———, 2020b, Elastic full waveform inversion with probabilistic petrophysical clustering: Geophysical Prospecting, **68**, no. 4, 1341 – 1355.

Asnaashari, A., R. Brossier, S. Garambois, F. Audebert, P. Thore, and J. Virieux, 2013, Regularized seismic full waveform inversion with prior model information: Geophysics, **78**, no. 2, R25–R36.

Fomel, S., P. Sava, I. Vlad, Y. Liu, and V. Bashkardin, 2013, Madagascar: open-source software project for multidimensional data analysis and reproducible computational experiments: Journal of Open Research Software, **1**.

Guitton, A., 2012, Blocky regularization schemes for full-waveform inversion: Geophysical Prospecting, **60**, 870–884.

Operto, S., Y. Gholami, V. Prieux, A. Ribodetti, R. Brossier, L. Metivier, and J. Virieux, 2013, A guided tour of multiparameter full-waveform inversion with multicomponent data: from theory to practice: The Leading Edge, **32**, no. 9, 1040–1054.

Plessix, R. E., 2006, A review of the adjoint-state method for computing the gradient of a functional with geophysical applications: Geophysical Journal International, **167**, no. 2, 495–503.

Tarantola, A., 1984, Inversion of seismic reflection data in the acoustic approximation: Geophysics, **49**, 1259–1266.

Virieux, J., and S. Operto, 2009, An overview of full-waveform inversion in exploration geophysics: Geophysics, **74**, no. 6, WCC1–WCC26.

Zhang, Z., and T. Alkhalifah, 2019, Regularized elastic full-waveform inversion using deep learning: Geophysics, **84**, no. 5, R741–R751.

Zhang, Z., T. Alkhalifah, E. Z. Naeini, and B. Sun, 2018, Multiparameter elastic full waveform inversion with facies-based constraints: Geophysical Journal International, **213**, 2112–2127.

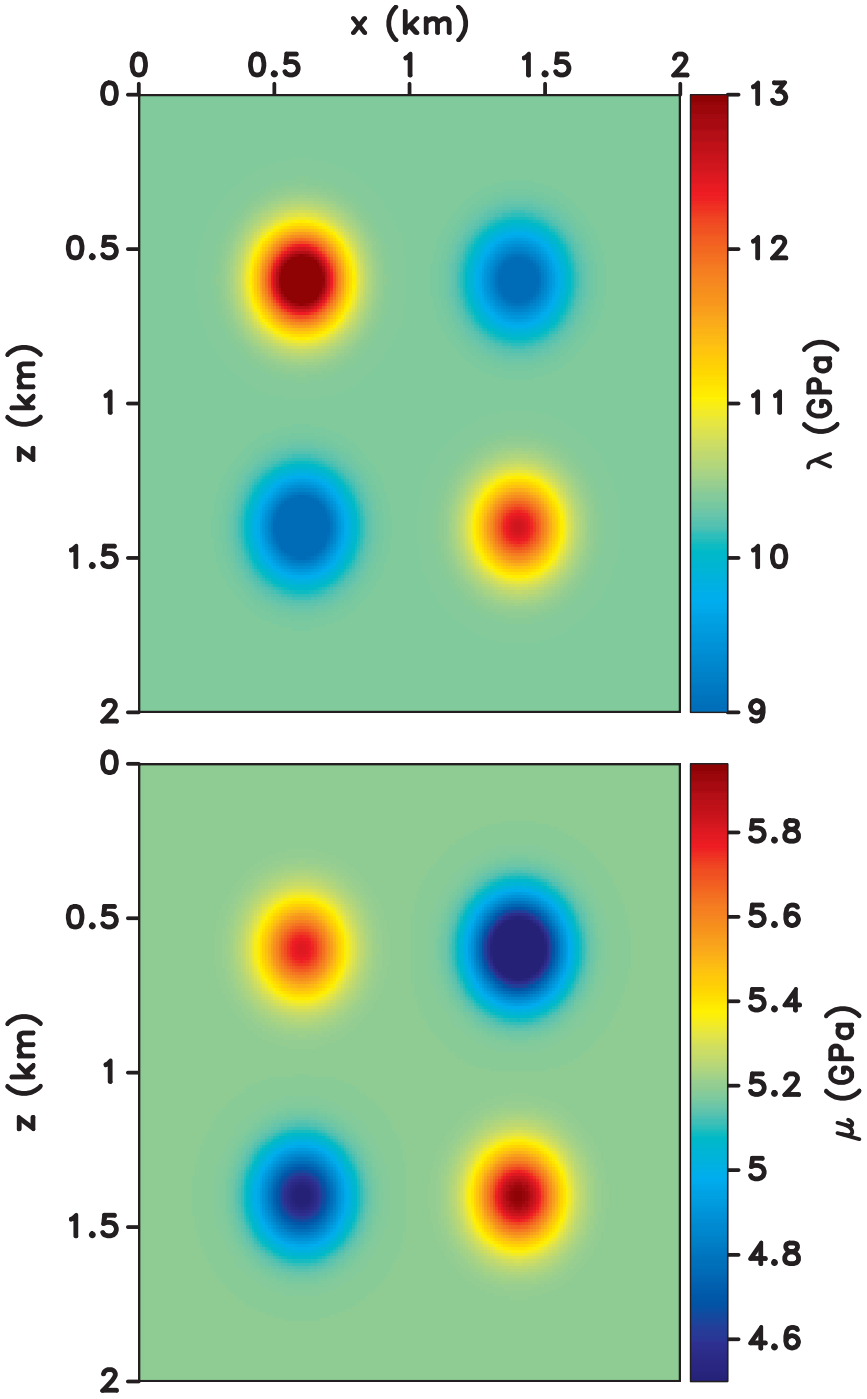


Figure 1. Synthetic models with four Gaussian anomalies for the λ and μ models centered at $(0.6, 0.6)$, $(1.4, 1.4)$ km, $(0.6, 1.4)$ and $(1.4, 0.6)$ km.

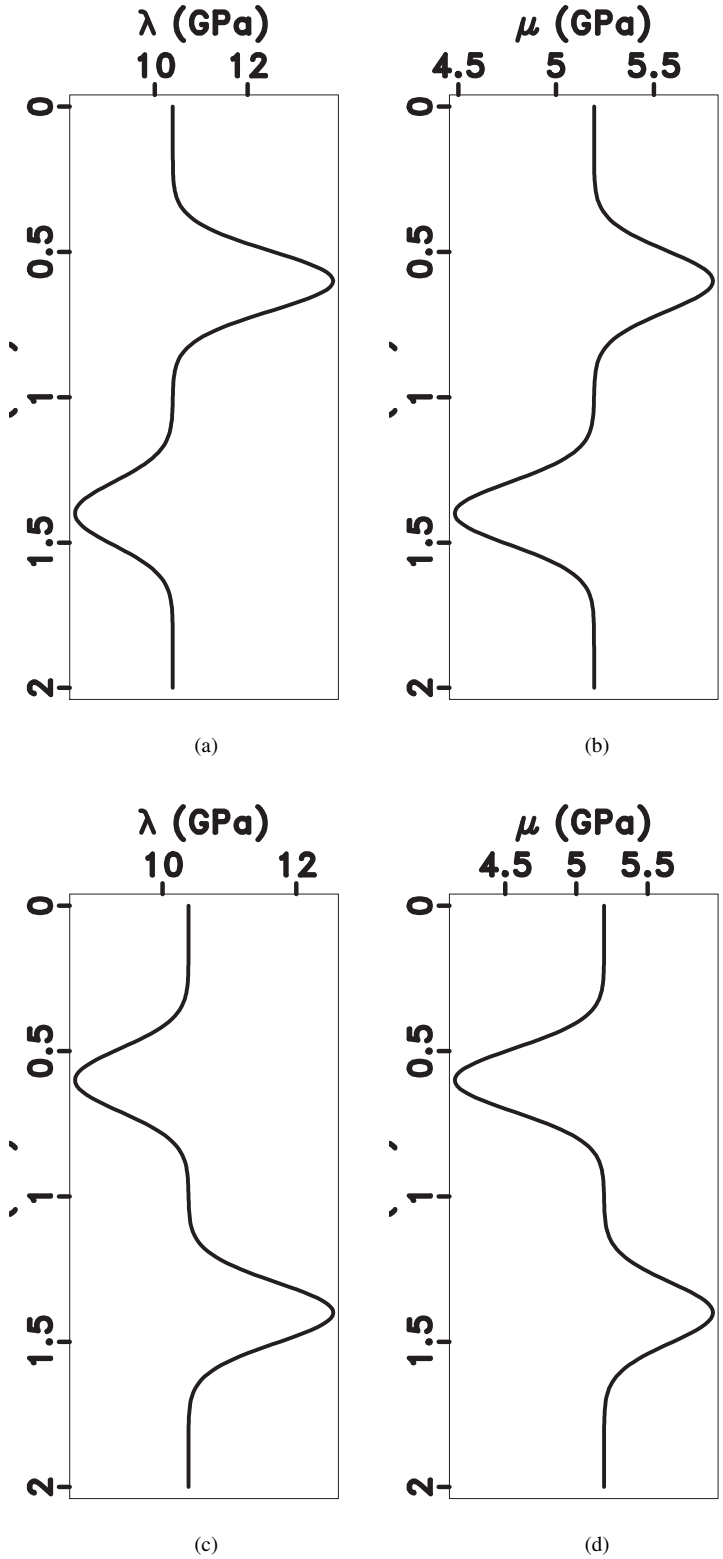


Figure 2. (a) λ and (b) μ logs extracted from the true models (Figure 1) at $x = 0.6$ km. (c) λ and (d) μ logs extracted from the true models (Figure 1) at $x = 1.4$ km.

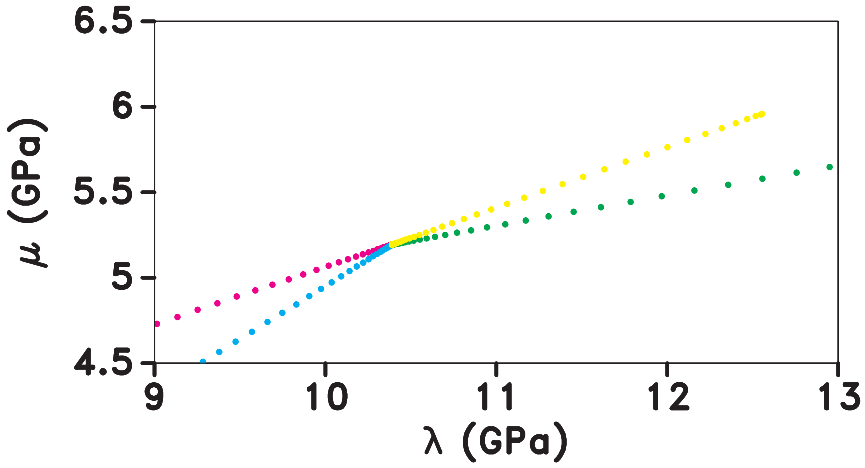


Figure 3. Crossplot of the well data used to calculate the PDFs for the penalty term in the FWI objective function. The different colors represent petrophysical data at different locations in the model, according to the well logs in Figure 2.

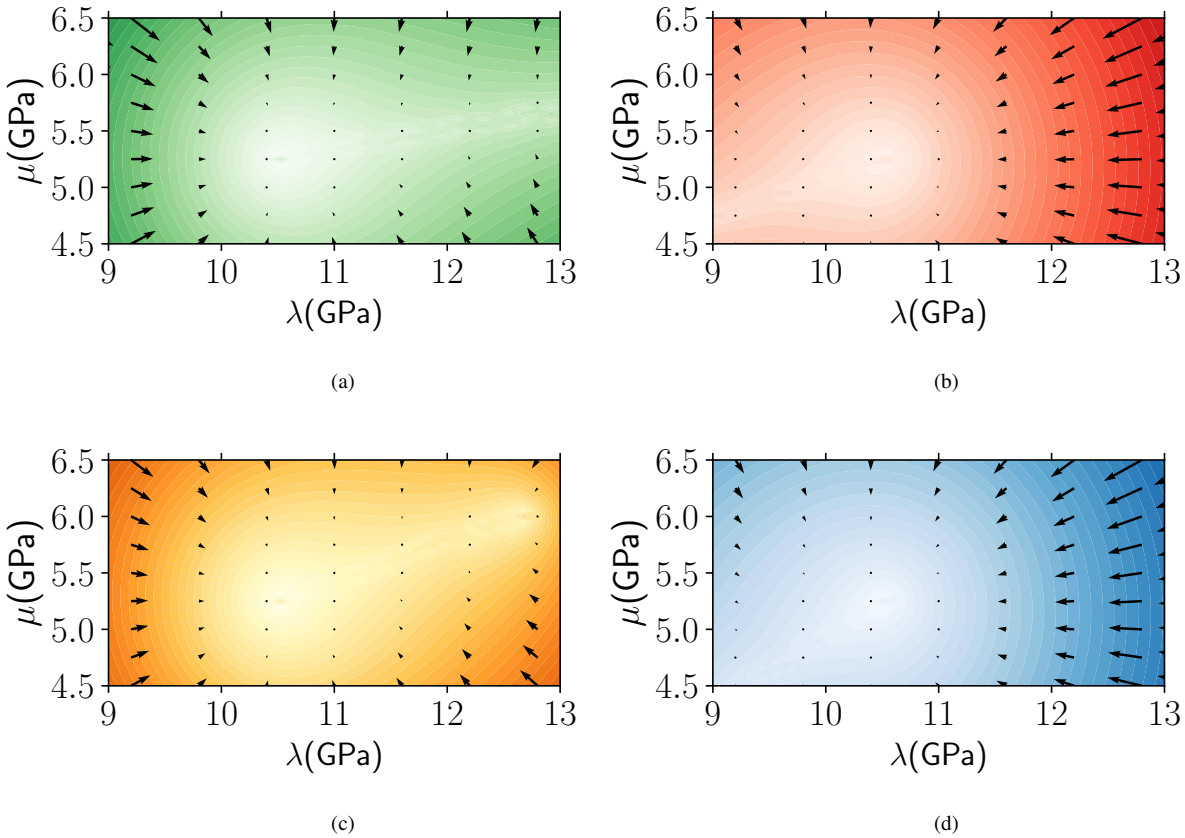


Figure 4. The distance $D(\mathbf{m})$ and its gradient for the the distributions (a) f_1, (b) f_2, (c) f_3, and (d) f_4.

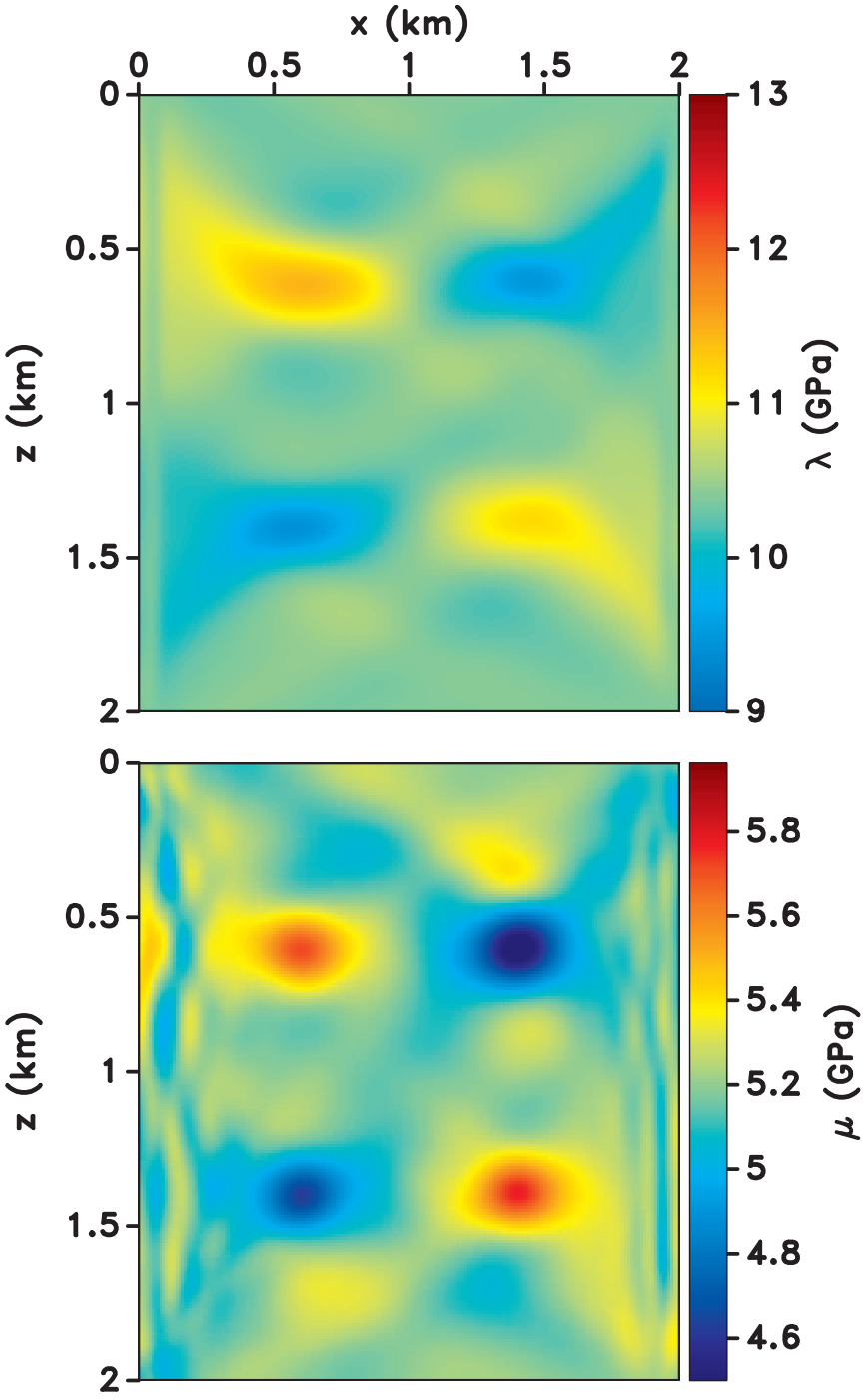


Figure 5. Recovered λ and μ models using the objective function $\mathcal{J}_D$.

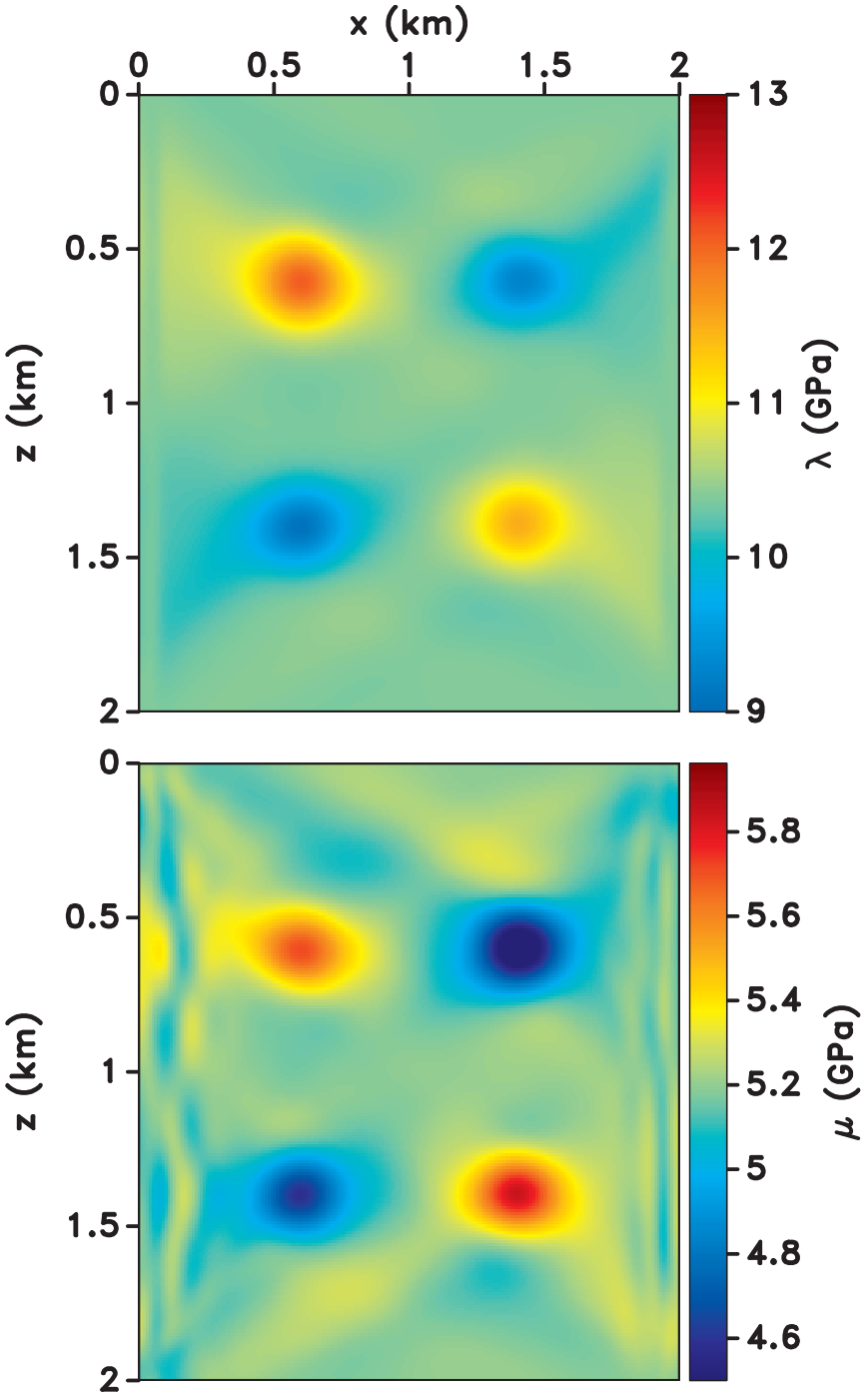


Figure 6. Recovered λ and μ models using the objective function $\mathcal{J}_D + \mathcal{J}_P$.

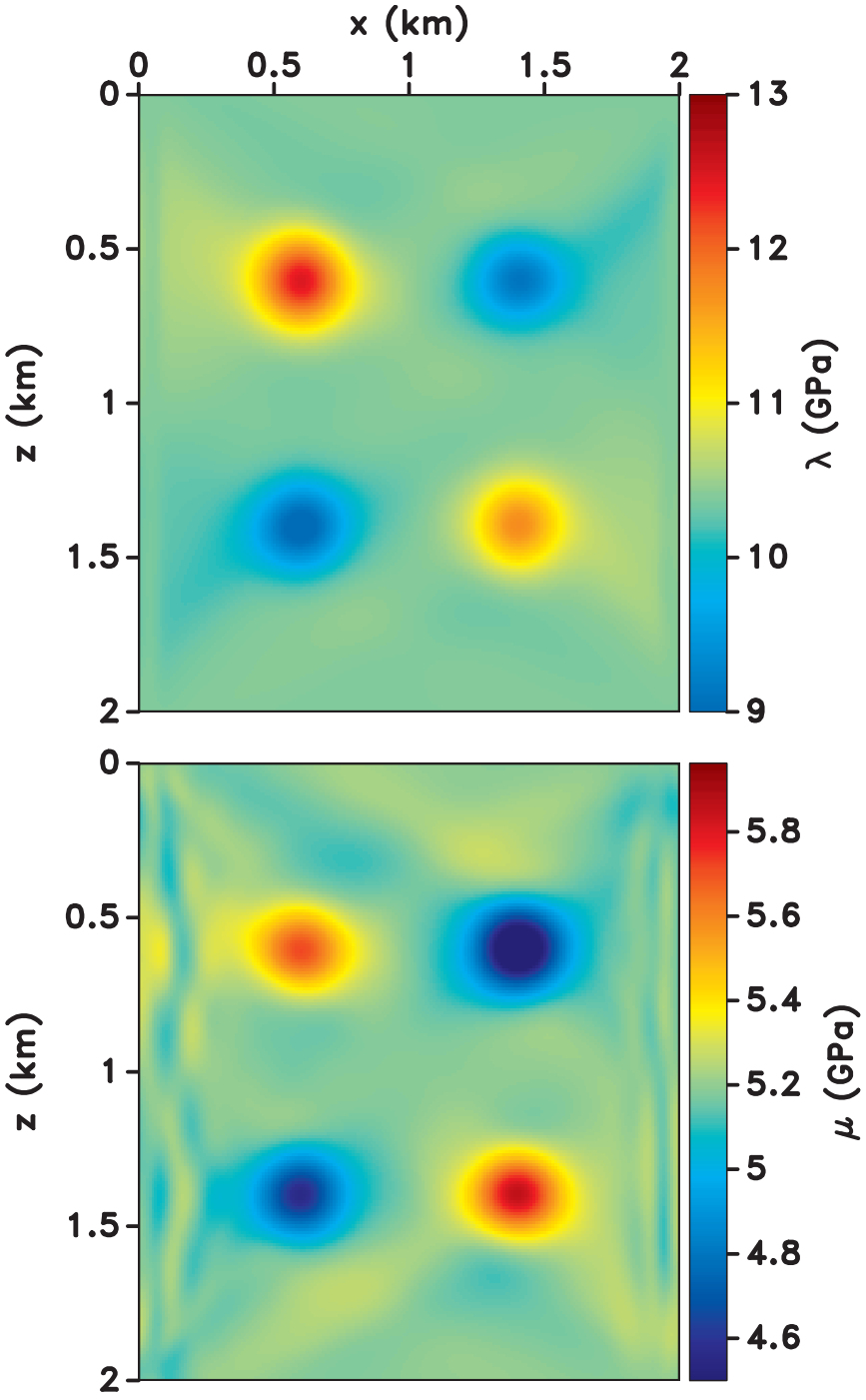


Figure 7. Recovered λ and μ models using the objective function $\mathcal{J}_D + \mathcal{J}_T$.